Thermal, dynamic-mechanical and electrical properties of UV-LED curable coatings containing porcupine-like carbon structures

Thermal, dynamic-mechanical and electrical properties of UV-LED curable coatings containing porcupine-like carbon structures

Rossella Arrigo [1,2], Mattia Bartoli [2,3], Daniele Torsello [3,4], Gianluca Ghigo [3,4], Giulio Malucelli [1,2]*

[1] Department of Applied Science and Technology, Viale Teresa Michel 5, 15121 Alessandria, Italy

[2] Consorzio Interuniversitario Nazionale per la Scienza e Tecnologia dei Materiali (INSTM), Via G. Giusti 9,50121 Florence, Italy

[3] Department of Applied Science and Technology, Politecnico di Torino Corso Duca degli Abruzzi 24, 10129 Torino

[4] Istituto Nazionale di Fisica Nucleare (INFN) Sez. Torino, Via P. Giuria 1, 10125 Torino, Italy

[*]Corresponding author: giulio.malucelli@polito.it; Tel.: +39-0131-229369

Abstract

In this work, multi-functional coatings based on a UV-LED curable epoxy-acrylate resin and different loadings (namely, 1, 2.5, 5 and 10 wt.%) of carbonaceous structures having a peculiar porcupine (PuP)-like morphology were formulated and thoroughly characterized through thermal, dynamic-mechanical and electrical analyses. More specifically, biochar-based particles derived from cellulose nanocrystals were modified through the growth of carbon nanofibers onto their outer surface, aiming at combining the effects of globular and high aspect ratio structures in a single filler. The preliminary characterization of the carbonaceous structures documented the achievement of a highly carbonized material involving spherical biochar particles having an average diameter ranging from 15 to 20 μm, covered by fibers displaying length up to 100 μm. As assessed by dynamic-mechanical characterization, the UV-LED cured composite films showed a progressive increase of the storage modulus values as a function of the amount of embedded PuP structures, indicating a strong level of interfacial interactions between the polymer network and the particles. Furthermore, the introduction of increasing amounts of PuPs induced a progressive increase of the material thermal conductivity (from 0.109 W/mK for unfilled cured resin, up to 0.161 W/mK, for the composite film containing 10 wt.% of filler) and a remarkable enhancement of the electrical conductivity (up to $(3.1\pm0.2)*10^{-2}$ S/m, for the composite film containing 10 wt.% of filler), thus pointing out the effectiveness of the proposed approach of surface modifying biochar particles in obtaining composite coating films with superior properties.

Keywords: UV-LED curing; epoxy-acrylate resin; biochar; thermal properties; electrical properties.

1. Introduction

From the last 10 years onwards, the industrial applications of UV curing processes exhibited a steadily growing trend, due to their high curing rate, reduced toxicity and lower environmental impact as compared to thermally-induced processes [1]. In fact, the use of a UV source to trigger the polymerization reactions allows minimizing the emissions of volatile organic compounds during the process [2]; furthermore, UV curing operations involve short reaction times and low energy consumptions, because of the possibility to complete the polymerization at room temperature by using proper UV sources [3,4]. Therefore, UV curing techniques have been exploited for a large variety of applications, ranging from the formulation of varnishes or protective coatings onto different substrates, to the fabrication of printed circuit boards for the electronic industry [5,6].

Usually, in traditional UV curing process, high-pressure mercury lamps are employed as radiation sources; however, these lamps reach very high temperatures during the process, thus limiting their suitability for temperature-sensitive substrates [7]; furthermore, the release of large amounts of heat, along with the production of ozone, contribute to increase the environmental impact of this technique [8].

Recent researches demonstrated that lower energy consumption and higher curing efficiencies can be achieved through the utilization of light emitting diodes (LEDs) as light sources for UV curing systems [9,10]. Compared to traditional UV lamps, UV-LED systems show longer full-intensity lifetime and improved electrical-to-optical conversion efficiency [11]. Additionally, due to the absence of emission in the infrared region, UV-LEDs deliver a cool radiation with respect to arc lamps, making the application of this technology suitable for heat-sensitive photocurable resins [12]. A major concern of UV-LED technique refers to the limited selection of suitable photoinitiators; in fact, UV-LED devices release an almost monochromatic light (usually at 365 or 395 nm), implying strict requirements on the absorption wavelength of the photoinitiator system [13].

Currently, researches concerning the utilization of UV-LED curing systems are mainly focused on the preparation of inks or photo-curable coatings [14,15], while a limited number of studies regarding the exploitation of this technique for the formulation of functional composite systems is reported in the literature [16,17]. In this context, in a previous work we investigated the preparation and characterization of epoxy-acrylate films containing different amounts of carbon-based micro- and nano-fillers (namely biochar (BC) and multi-walled carbon nanotubes) and obtained by means of UV-LED curing [18]. The characterization of the obtained films proved the completeness of the photopolymerization reactions even for the composites containing high loadings (up to 1 wt.%) of the fillers, demonstrating the suitability of UV-LED process for the preparation of composite coatings. Additionally, a beneficial effect of the biochar presence on the extent of dispersion of carbon

nanotubes was observed; more specifically, owing to their peculiar structure and morphology, biochar particles were able to exert a "shuttle effect" towards carbon nanotubes, thus promoting the achievement of a homogeneous dispersion of the nanofillers within the host matrix.

At present, the exploitation of biochar as filler for thermoplastics- and thermosets-based composites is attracting a great interest, due to its intriguing characteristics (such as excellent electrical properties and large surface area) and high environmental sustainability [19-21]. Besides, the possibility to obtain BC particles having different characteristics, in terms of internal porosity and presence of functional groups on their surface, through the optimization of the productive process, allows adapting the BC properties to the selected polymeric matrix, leading to the achievement of high-performance composite materials [22,23]. BC is usually derived from the thermo-mechanical conversion in oxygen-limited environment of agricultural [24,25] or post-industrial and municipal wastes [26], showing a great potential in the formulation of eco-friendly commercial goods, in the framework of the general circular economy approach [27].

In this work, we propose an innovative approach to modify the morphology of BC-based particles derived from cellulose nanocrystals (CNCs) through the growth of carbon nanofibers onto their outer surface. This leads to the formation of porcupine-like arrangements that, thanks to their peculiar morphology, may combine the effects provided by either globular or high aspect ratio carbon structures in a single filler. For this purpose, the porcupine (PuP)-like structures were then dispersed in a UV-LED curable epoxy-acrylate resin at different loadings (ranging from 1 to 10 wt.%), aiming at obtaining multi-functional coatings with enhanced final properties. In particular, the structure-properties relationships of the formulated films were assessed, also considering the effect of the embedded particles on the thermal and electrical properties of the cured resin.

2. Materials and Methods

2.1 Materials

A commercially available epoxy-acrylate resin, Ebecryl 150 (Bisphenol-A-ethoxylate-diacrylate, hereinafter coded as EB) was kindly supplied by Allnex (Brussels, Belgium). 2,4,6-Trimethylbenzoyl-diphenylphosphineoxide, herein after coded as TPO, was kindly supplied by IGM Resins (Mortara, Italy) and used as photoinitiator for the UV-LED curing process.

CNCs were purchased from Alberta-Pacific Forest Industries (Batch COMP170823-H) and used as received without any purification. Oleic acid (> 98%) was purchased by Sigma-Aldrich and used without any further purification. CNCs were produced through an acid hydrolysis of waste wood pulp by using sulphuric acid and isolated though precipitation and filtration. Prior pyrolysis, neat CNCs

aggregated in round-shape bundles of about 20 μm of average diameter. The surface residual sulfonic groups were removed during the pyrolytic process as reported in [28].

2.2 Preparation of particles

CNCs were mixed with oleic acid at 1:1 weight ratio. The mixture was placed into a steel vessel and put into a pre-heated a tubular furnace (Carbolite TZF 12/65/550), in nitrogen atmosphere at 1000°C for 30 min. Afterwards, the resulting biochar was removed and rapidly cooled down at room temperature.

2.3 Preparation of the UV-LED curable mixtures

The carbonaceous particles were dispersed in EB with final concentrations of 1, 2.5, 5 and 10 wt.%, using a tip Sonics Vibra-cell ultrasonicator (300 W power, from Sonics & Materials, Inc. Newtown, USA) for 15 minutes. In order to avoid the instantaneous temperature rise, ultrasounds were pulsed with cycles of 10 s alternated to 10 s pause to favor a better heat diffusion [29]. Then, 6 wt.% of TPO was added to the UV-LED curable mixture and the dispersions were coated on glass plates using proper wire-wound applicators for obtaining about 200 μm thick coatings suitable for the successive characterizations. The coated glass plates were then subjected to the UV-LED curing process, using a Heraeus Noblelight UV-LED NC1 unit (Cambridge, UK), working in dynamic conditions (belt speed: 1 m/min), at 395 nm, with a radiation intensity on the sample surface of about 4.8 W/cm^2; the energy density (i.e. dose) was around 10 J/cm^2.

2.4 Characterization techniques

Rheological measurements were performed on the EB-PuP liquid dispersions using an ARES (TA Instrument, USA) strain-controlled rheometer in parallel plate geometry (plate diameter: 50 mm). The complex viscosity was measured performing frequency scans from 10^{-2} to 10^2 rad/s at 25 °C. The strain amplitude was selected for each sample in order to fall in the linear viscoelastic region.

Microstructures were observed using a Scanning Electron Microscope SEM Zeiss (Oberkochen, Germany) (beam voltage: 20 kV) on the cross-sections of the investigated samples fractured in liquid nitrogen. Before the observations, the fracture surfaces were gold metallized.

Differential scanning calorimetry (DSC) analyses were performed using a QA1000 TA Instrument apparatus (TA Instrument Inc., Waters LLC, USA). All the experiments were performed under dry N_2 gas (flow: 50 mL/min) using samples of about 10 mg in sealed aluminum pans. All the films underwent the following cycle: (1) heating from 0 °C to 160 °C at 10 °C/min; (2) cooling down to 0 °C at 10 °C/min; and (3) heating from 0 °C to 160 °C at 10 °C/min.

Raman spectra were collected using a Renishaw inVia (H43662 model, Gloucestershire, UK) equipped with a green laser line (514 nm) with a 50× objective. Raman spectra were recorded in the range from 250 cm^{-1} to 3500 cm^{-1}.

Thermogravimetric analyses (TGA) were performed using a Discovery apparatus (TA Instruments, USA) (experimental error: ±0.5 wt%, ±1 °C). Samples (about 10 mg) were placed in alumina pans and runs were carried out in the range 50-700 °C, with a heating rate of 10 °C/min, under both nitrogen and air flow (35 and 25 ml/min, respectively). $T_{5\%}$, $T_{10\%}$ (i.e., the temperatures, at which 5% or 10% weight loss, respectively, occurs), and T_{max} values (i.e. the temperatures corresponding to the peaks appearing in dTG curves) were calculated; besides, the final residue at 700 °C was measured.

UV-Vis spectroscopy measurements were performed on the UV-LED cured films by using a Shimadzu UV-Vis spectrophotometer UV2600 series (Shimadzu Italia Srl, Milano, Italy); wavelength range was set between 200 and 800 nm.

Dynamic-mechanical measurements (DMA) tests were performed using a Q800 TA Instrument (TA Instruments Inc., New Castle, DE, USA) in tensile configuration. The following experimental conditions were adopted: temperature range from 30 to 120 °C, heating rate of 5 °C/min, 1 Hz frequency and 0.05% of oscillation amplitude in strain-controlled mode. For each material, the tests were carried out on three different samples and the results averaged.

Thermal conductivity measurements were carried out with a TPS 2500S apparatus (Hot Disk AB, Göteborg, Sweden), equipped with a Kapton sensor (radius 3.189 mm), using the transient plane source (TPS) method [30]. The test temperature (23.00 ± 0.01 °C) was controlled by a silicon oil bath (Haake A40, Thermo Scientific Inc., Austin, USA) equipped with a temperature controller (Haake AC200, Thermo Scientific Inc., Austin USA).

DC electrical measurements were performed on each thin film sample at room pressure, following the method described in [31]. The complex permittivity of the samples was measured in the 1-12 GHz range by means of a cylindrical coaxial cell (EpsiMu toolkit [32]), placing the sample as a dielectric spacer between inner and outer conductors. The internal and external cell diameters are 0.6 cm and 1.3 cm, respectively. Two conical parts link the cell to standard connectors, keeping the characteristic impedance at 50 Ω, thus minimizing mismatch and energy losses. The system is connected to a Rohde Schwarz ZVK Vector Network Analyzer, suitably calibrated, and measurements are analyzed with a two-port transmission line technique. The imaginary part of the dielectric permittivity is related to the AC conductivity σ by $\varepsilon'' = \left(\frac{\sigma}{\omega\varepsilon_0} + \varepsilon_d''\right)$, where the σ term is dominant for frequencies ω in the microwave range. In order to perform the measurement, the samples were geometrized by hand to fit the coaxial measurement cell. Due to the extremely small thickness of the studied films, for each composition several samples obtained from the same film were stacked in the measurement cell to

achieve a clean signal (after checking that upon varying the number of stacked films, the obtained values of complex permittivity did not change).

3. Results and Discussion

3.1 Characterization of PuP particles

The shape tunability of CNCs was previously discussed by Bartoli et al. [28], showing a wide spectrum of morphologies ranging from deformed spheres to needles. Here, we approached carbonized CNCs for the production of carbon nanofibers tailored spheres treated at 1000°C. High temperature produced BC displaying interesting features for the production of conductive composites [33], but pristine BC produced from CNCs was recovered as spherical particles that induced the lower performances for electrical conductivity. Accordingly, we tuned the production of BC aiming to obtain fiber decorated particles as schematized in Figure 1.

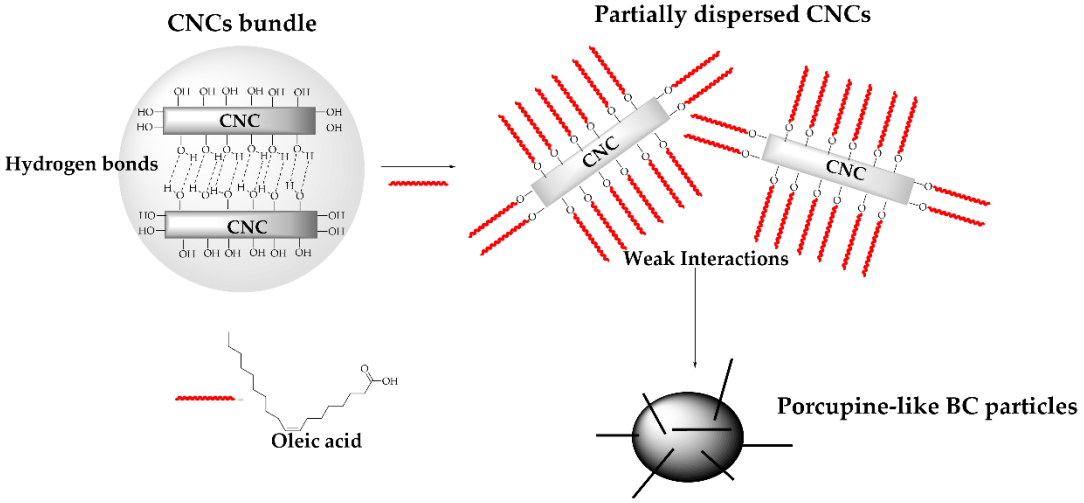

Figure 1. Schematic representation of PuP particles production

By using oleic acid, we promoted the partial breaking of the hydrogen bonds network, which induce the regrouping of CNCs into spherical bundles due to the esterification of hydroxylic functionalities. After the carbonization reactions, the surface tailored CNCs turned into porcupine-like materials as shown in the SEM pictures of Figure 2 (a and b).

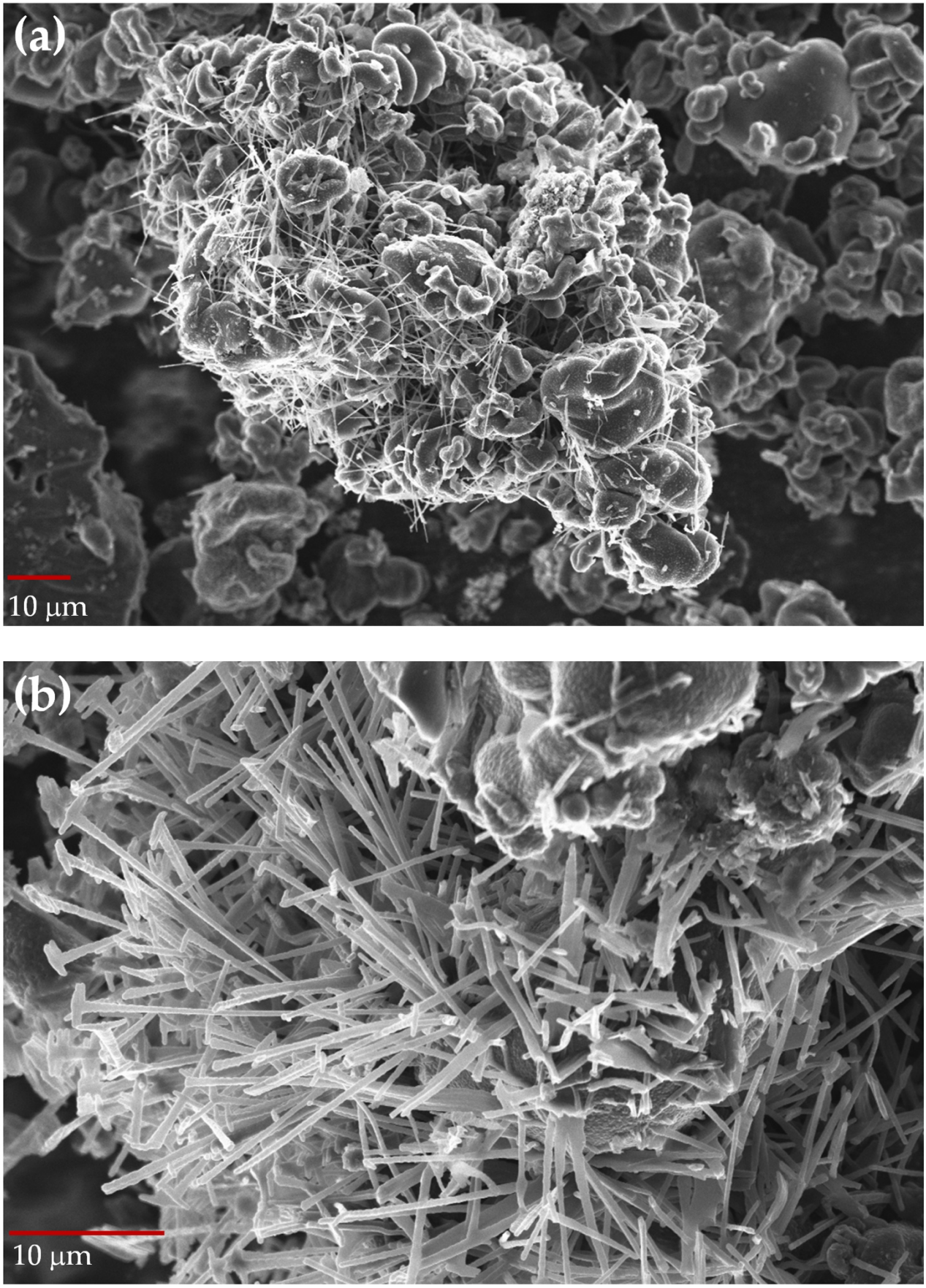

Figure 2. SEM pictures of PuP structures at different magnifications

Spherical BC particles appeared as cluster of dozen of particles with an average diameter ranging from 15 µm to 20 µm covered by fibrous carbonized CNCs. Fibrous materials displayed a length of up to 100 µm and an average diameter around 250 nm. This material was highly carbonized as shown by the Raman spectrum reported in Figure 3.

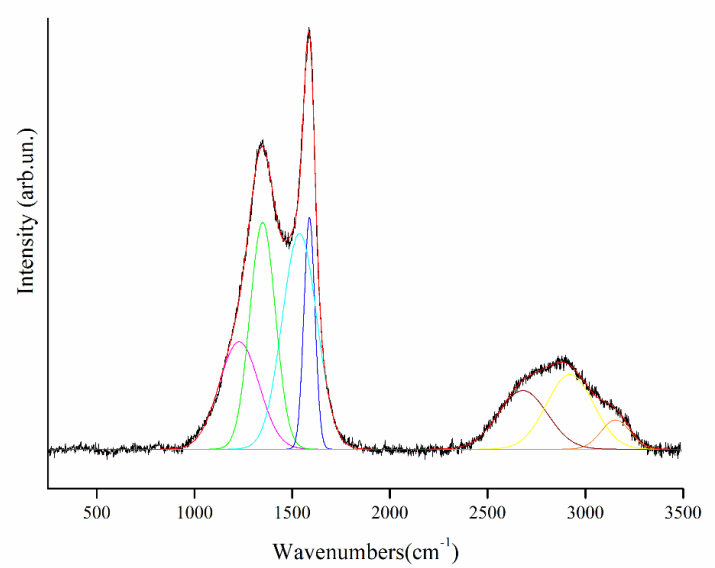

Figure 3. Raman spectra of PuP particles. In black is reported the original signal, in red the fitted one and in the other colors each fitting component.

Raman spectrum confirmed the obtainment of a material still far away from a complete graphitization, but with an I_D/I_G ratio of 0.83 that was significantly lower than BC obtained at 1000°C [34]. This could be ascribed to the fast aromatization of cellulose under pyrolytic conditions [35], which led to a more efficient reorganization of the graphitic domains.

Nonetheless, the graphitization was to be completed as clearly shown by TGA analysis of BC particles reported in Figure 4.

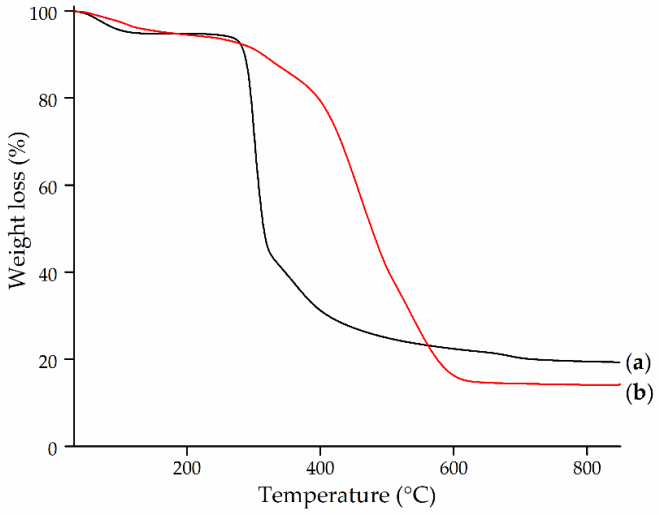

Figure 4. TGA of (a) neat CNCs and (b) PuP particles in nitrogen atmosphere.

Pristine CNCs (Figure 4 a) displayed a 5 wt.% loss at about 100°C due to water release and a main degradation stage around 250°C as consequence of cleavage of β 1,4-glycosidic bond of glucose chains. The degradation of PuP involves a multi-step mechanism: in particular, PuP starts degrading at 110°C due to the water loss. Then, the degradation of carboxylic functionalities present as a consequence of oleic acid additions occurs at about 275°C. The estimation of residual carboxylic groups is around 3 wt.%. An additional degradation step takes place at about 560°C and involves the fibrous part of PuP (around 8 wt.% of the PuP structures).

3.2 Rheological behavior of EB-PuP mixtures

Figure 5 reports the complex viscosity curves as a function of the frequency for unfilled EB and PuP-containing liquid mixtures. Neat EB exhibits a Newtonian rheological behavior, involving an almost frequency-independent complex viscosity, in the whole tested frequency interval. The incorporation of increasing loadings of PuP particles causes a progressive rise of the complex viscosity values, especially in the very low frequency region, where the response of large portions of oligomeric chains is recorded. In fact, in the lowest tested frequency interval, PuP-containing dispersions show an apparent yield stress behavior, attributable to a restriction of the macromolecular dynamics resulting from the established interactions between the oligomeric chains and the embedded particles. In a previous work [18], we have reported a lubricant action exerted by the introduced BC in EB-BC mixtures, causing a progressive decrease of the viscosity values of the dispersions with increasing the loading of the embedded particles. The different behavior observed for the PuP-containing systems can be ascribed to the peculiar porcupine-like morphology of the filler, which causes the formation of a highly entangled structure, involving the establishment of strong interactions between the EB chains and the carbon nanofibers, hence hindering the motion of the EB oligomeric chains and preventing their complete relaxation.

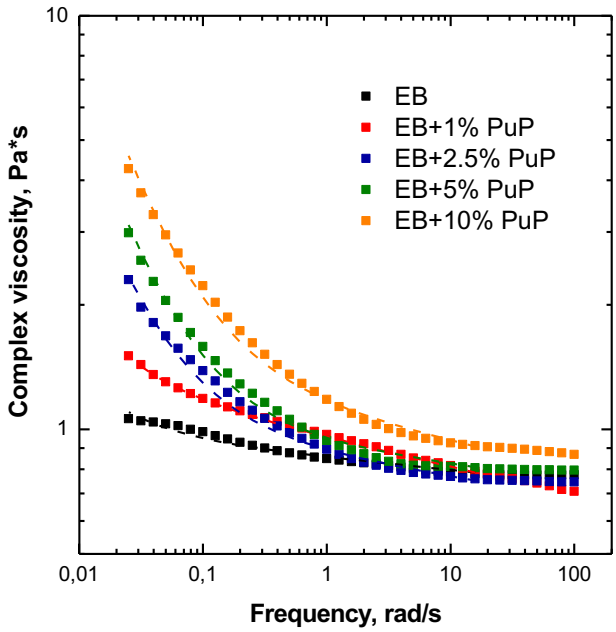

Figure 5. Complex viscosity curves for unfilled EB and PuP-containing mixtures.

3.3 Morphological study of UV-LED cured EB-PuP films

EB-PuP thin films were preliminary studied through SEM analyses as presented in Figure 6. The films increase their thickness as a result of the introduction of increasing loadings of PuP particles due to the higher viscosity of the composite systems, slightly affecting their processability. The average thickness of the films ranged from 80 μm (Figure 6 a) up to 200 μm (Figure 6 g). Spherical particles were dispersed quite well and formed clusters at high loading as shown in Figure 6 e and g. Fibrous particles were dispersed quite well and they are hardly detectable.

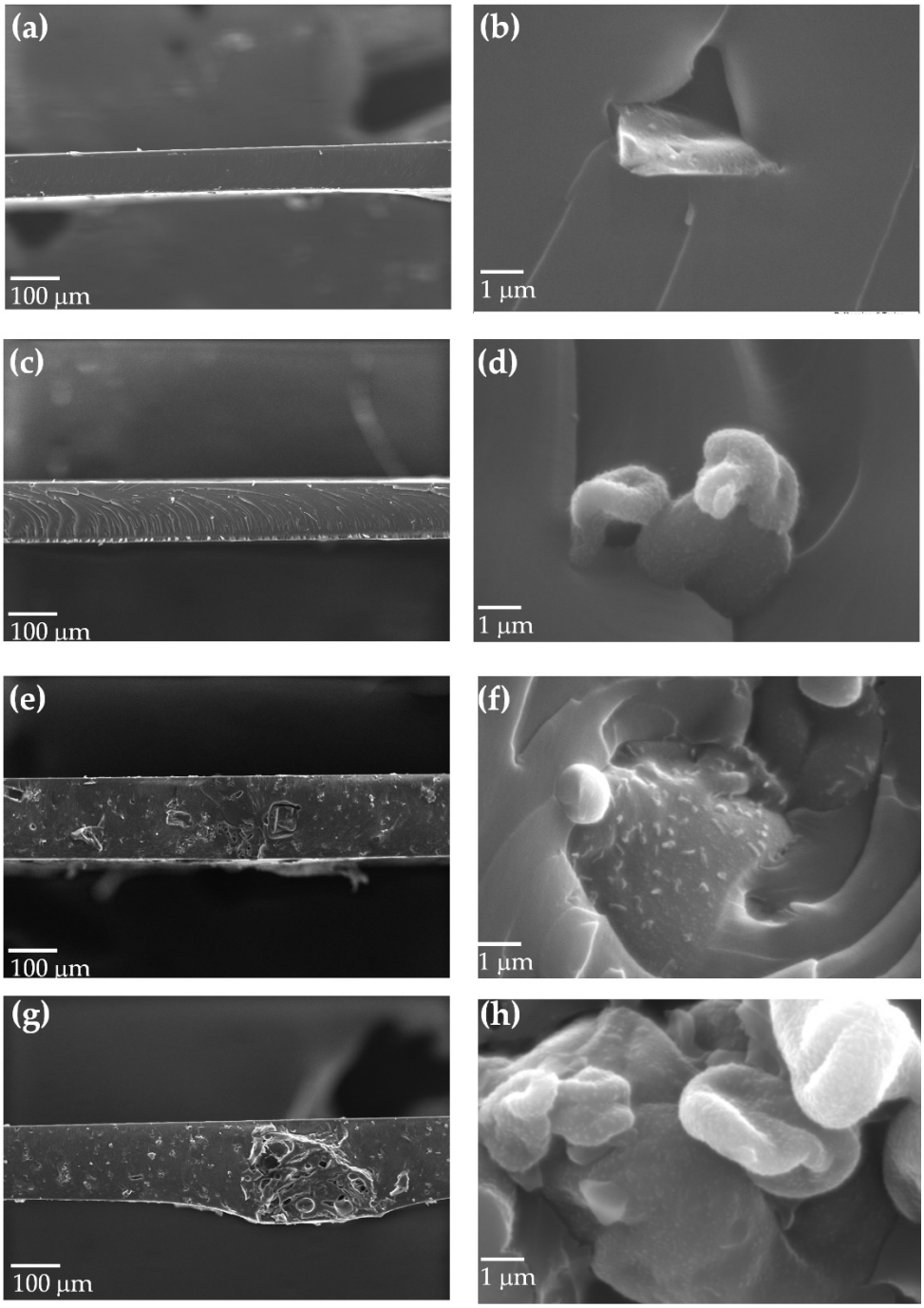

Figure 6. SEM of films containing (**a** and **b**) 1 wt.%, (**c** and **d**) 2.5 wt.%, (**e** and **f**) 5 wt.% and (**g** and **h**) 10 wt.% of PuP.

3.4 Thermal properties of UV-LED cured EB-PuP films

First, DSC measurements were carried out on cured EB and PuP-containing films aiming at verifying the completeness of the UV-LED curing process through the absence of any exothermic peak in the first heating up scan; furthermore, results coming from DSC tests were used to assess the possible effect of the incorporated particles on the thermal behavior of the composite films, and in particular

on their Tg (glass transition) values. In Figure 7 a-b, the thermograms recorded during the first and second heating scan respectively, are plotted; besides, the T_g values, evaluated at the midpoint of heat capacity steps, are reported.

Looking at the DSC traces recorded during the first heating run (Figure 7a), the presence of an endothermic peak that superimposes to the specific heat step associated with the glass transition of the polymer network can be observed for either unfilled or composite films. This peak can be associated to an enthalpy relaxation attributable to the non-equilibrium thermodynamic state, in which the macromolecules are frozen due to the fast UV-LED curing process [36]. Besides, for all the investigated materials no exothermic phenomena are observed above the glass transition temperature, hence indicating the effectiveness of the experimental conditions adopted for the UV-LED curing process in promoting the formation of a fully cured network, also in presence of high loadings of PuP particles.

In the second heating scan (Figure 7b), due to the heating at temperatures above T_g and the subsequent cooling down that the polymer network underwent during the measurement, the macromolecular chains can reach a more stable conformation: this phenomenon causes the disappearance of the enthalpy relaxation. Besides, a negligible effect of the embedded PuP particles on the glass transition of EB can be observed, as the calculated T_g values for all investigated materials range from 69 to 73 °C.

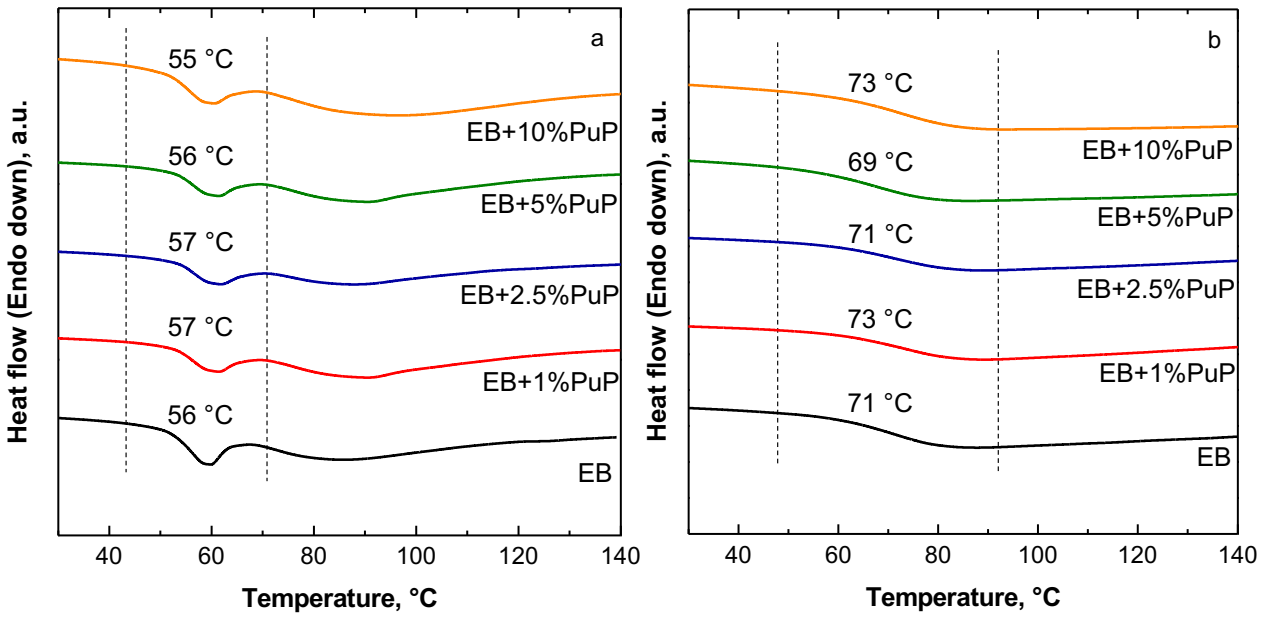

Figure 7. DSC thermograms recorded during the (a) first and (b) second heating scan for all investigated materials.

In order to assess the possible effect of PuP particles on the thermal and thermo-oxidative stability of the UV-LED cured films, thermogravimetric analyses were performed, under both nitrogen and air

atmospheres; the collected results are listed in Table 1. In nitrogen, the degradation of all investigated materials occurs in a single step. The presence of PuP particles induces a slight anticipation of the EB degradation phenomena; in fact, a progressive decrease of $T_{5\%}$ and $T_{10\%}$ values as a function of the particle loading can be noticed, along with a shift towards lower temperature values of the maximum degradation temperature, probably due to the catalytic effect exerted by the residual carboxylic groups on the particle surface, notwithstanding a monotonic increase of the residues of the composite films at the end of the analyses with increasing the amount of embedded PuP particles.

Conversely, in air, the degradation mechanism involves three main steps: the first one (at about 375 °C) related to the degradation of low molecular weight structures, the second one (occurring in a range between 400 and 500 °C) attributable to the main degradation of the polymer network and the last one (at about 550°C) associated with the further oxidization of the degradation species produced during the previous stages. As far as the effect of embedded PuP particles is concerned, the obtained results suggest that the thermo-oxidative stability of the composite films is almost unchanged as compared to that of unfilled EB; in fact, regardless of the PuP loading, no remarkable changes of the values of the typical degradation temperatures are noticed, notwithstanding that higher residues at the end of the test are obtained for the composites.

Table 1. Thermal and thermo-oxidative stability of unfilled EB and PuP-containing composite films.

	N_2				***Air***					
	$T_{5\%}$ [°C]	**$T_{10\%}$ [°C]**	**T_{max} [°C]**	**Residue at 700°C [%]**	**$T_{5\%}$ [°C]**	**$T_{10\%}$ [°C]**	**T_{1max} [°C]**	**T_{2max} [°C]**	**T_{3max} [°C]**	**Residue at 700°C [%]**
EB150	369	395	441	2.7	318	352	383	433	553	0
EB150+1%PuP	363	394	438	3.3	321	356	379	432	561	0.1
EB150+2.5%PuP	345	379	421	5.0	306	340	371	428	545	0.3
EB150+5%PuP	327	372	426	10.5	296	342	362	425	543	0.6
EB150+10%PuP	342	371	421	16.7	326	354	364	426	548	1.9

Figure 8 shows the thermal conductivity data of unfilled EB cured film and of all investigated composites as a function of the amount of PuP particles. From an overall point of view, the introduction of increasing amounts of PuPs induces a progressive increase of the material thermal conductivity. The observed trend seems to indicate a homogeneous dispersion of the particles within the polymer network, confirming the morphological observations. Differently to what was observed

for similar composite films containing BC particles and multi-walled carbon nanotubes, for which the clustering phenomena of the embedded nanofillers caused a monotonic decrease of the thermal conductivity for filler loadings beyond 0.01 wt.% [18], the anchoring of carbon fibers onto the BC surface promotes a more uniform particle dispersion, preventing the filler agglomeration and inducing increased thermal conductivity values.

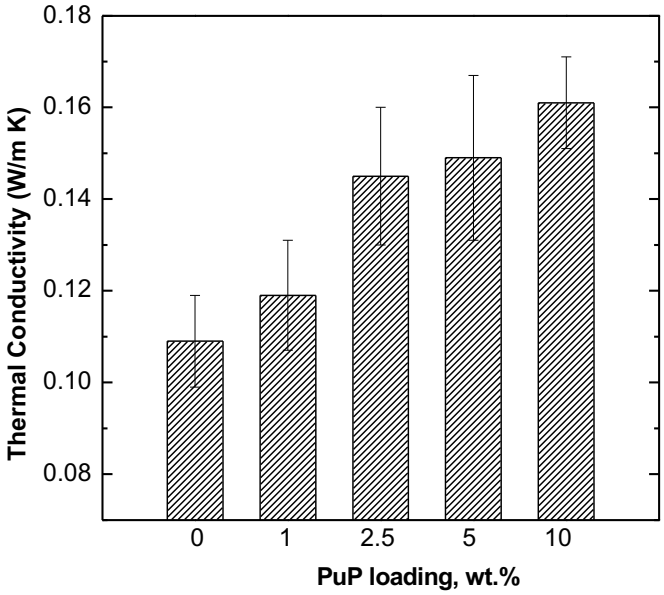

Figure 8. Thermal conductivity of UV-LED cured EB and its composite films as a function of filler loading.

3.5 Dynamic-mechanical properties of UV-LED cured EB-PuP films

Figure 9 presents the results from dynamic-mechanical analyses, in terms of storage modulus and tanδ as a function of temperature for all the investigated UV-LED cured films. Looking at the curves reported in Figure 9a, a progressive increase of the storage modulus values with increasing the loading of PuP particles can be noticed, especially in the glassy region. Concerning the tanδ curves, the composite films exhibit slightly higher glass transition temperature values as compared to the unfilled counterpart; besides, a progressive decrease of the peak intensity can be noticed with increasing the particle loading.

These findings can be related to the strong level of interfacial interactions taking place between the oligomeric chains and the introduced PuP particles; in fact, the embedded particles are able to restrict the segmental dynamics of the polymeric phase located in the interfacial region, causing a progressive shift of the glass transition temperature values towards higher temperatures as a function of particle loading [37]. Furthermore, the restriction of the segmental chain motion induces an increased elasticity; as a result, a lower extent of energy is dissipated during the mechanical test and this phenomenon causes the lowering of the peak intensity [38].

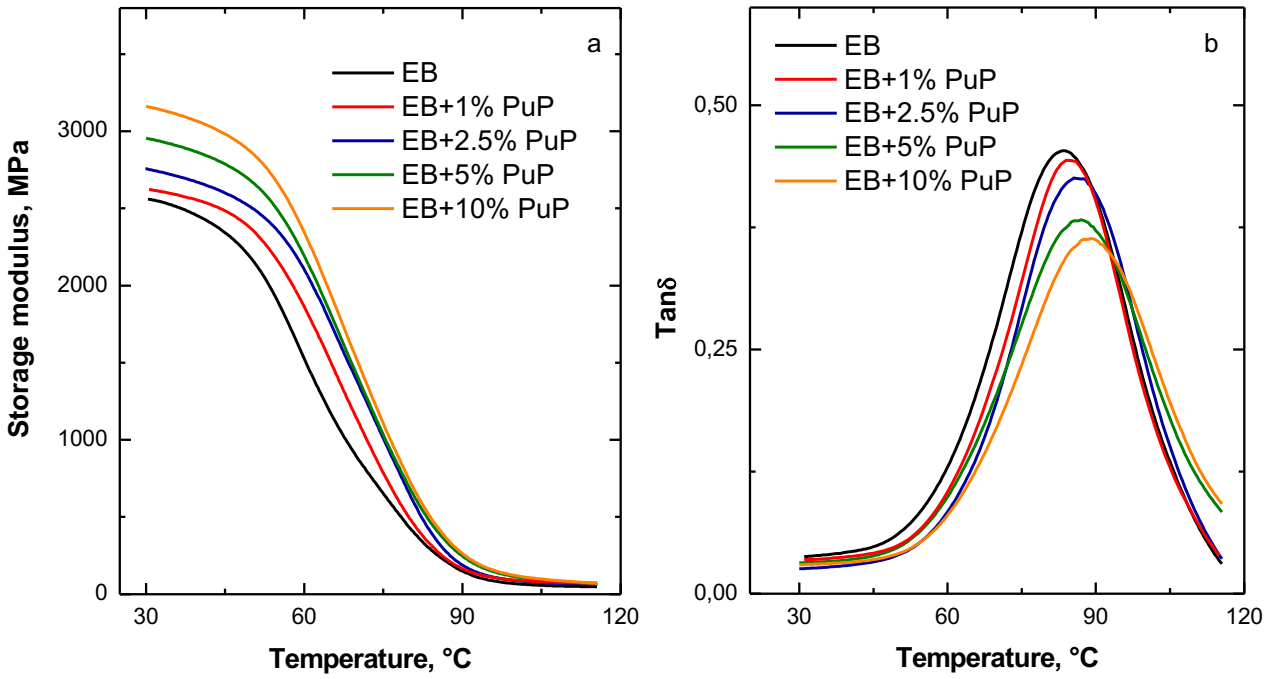

Figure 9. (a) Storage modulus and (b) tanδ as a function of temperature for all investigated materials.

3.6 Optical properties of UV-LED cured EB-PuP films

With the aim of assessing the influence of the embedded PuP particles on the optical properties of the UV-LED cured films, UV-Vis spectroscopy measurements were performed; the obtained spectra are plotted in Figure 10. A remarkable effect of the presence of PuP particles on the transmittance of the composite films can be clearly noticed. More specifically, the composite film containing 1 wt.% of PuP particles exhibits a slightly decreased transparency as compared to the unfilled counterpart, suggesting a good optical homogeneity resulting from an uniform distribution of the particles within the cured network. For the films containing higher PuP particle loadings, the transparency significantly reduces, likely due to either the light scattering provided by the carbon nanotubes or the occurrence of some clustering phenomena. We have previously demonstrated [18] that the simultaneous presence of biochar particles and multi-walled carbon nanotubes in EB-based UV-LED cured films caused a significant reduction of the film transmittance at low filler loading (i.e. 1 wt.%), due to the light scattering phenomena provided by the nanofillers. The results obtained in the present work indicate that the transmittance of the composite films is dramatically reduced only at very high particle loadings (i.e. 5 and 10 wt.%), pointing out that the proposed strategy of surface modifying biochar particles is very effective in keeping a high transparency in the resulting composite films.

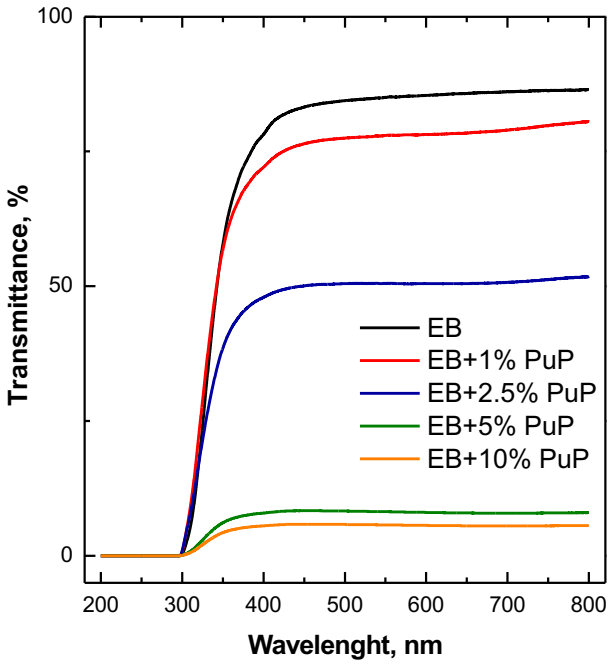

Figure 10. UV-Vis spectra of EB-based films.

3.6 Electrical properties of UV-LED cured EB+PuP films

DC measurements on thin films showed a too low conductivity for samples containing up to 1 wt.% of PuP. By increasing the PuP loading to 2.5 wt.%, a low conductivity up to $(2.9\pm0.1)*10^{-4}$ S/m was detected. Higher PuP loadings (namely, 5 and 10 wt.%) increased the conductivity values up to around $(1.3\pm0.1)\ 10^{-2}$ S/m and $(3.1\pm0.2\ )*10^{-2}$ S/m, respectively. Considering the temperature used for the production of PuP structures, these values are quite high as compared with those achieved by using coffee derived biochar at same loading [31] and comparable with those measured by using thermal annealed wood derived biochar [39].

The high frequency characterization is shown in Figure 11: a monotonic increase of both the real part of the complex dielectric permittivity ε' and of the AC conductivity σ with PuP loading is found when a sufficient filler content was added to EB. In particular, the curves for 1 wt.% and 2.5 wt.% are not shown because they superimpose with that of the pure EB samples. The investigated frequency range covers the S (2-4 GHz), C (4-8 GHz) and X (8-12 GHz) microwave bands employed for radars, satellite communications and wireless computer networks. While ε' is quite constant in the investigated frequency range for all samples, the conductivity strongly increases with frequency, making these materials interesting for applications in the communications field.

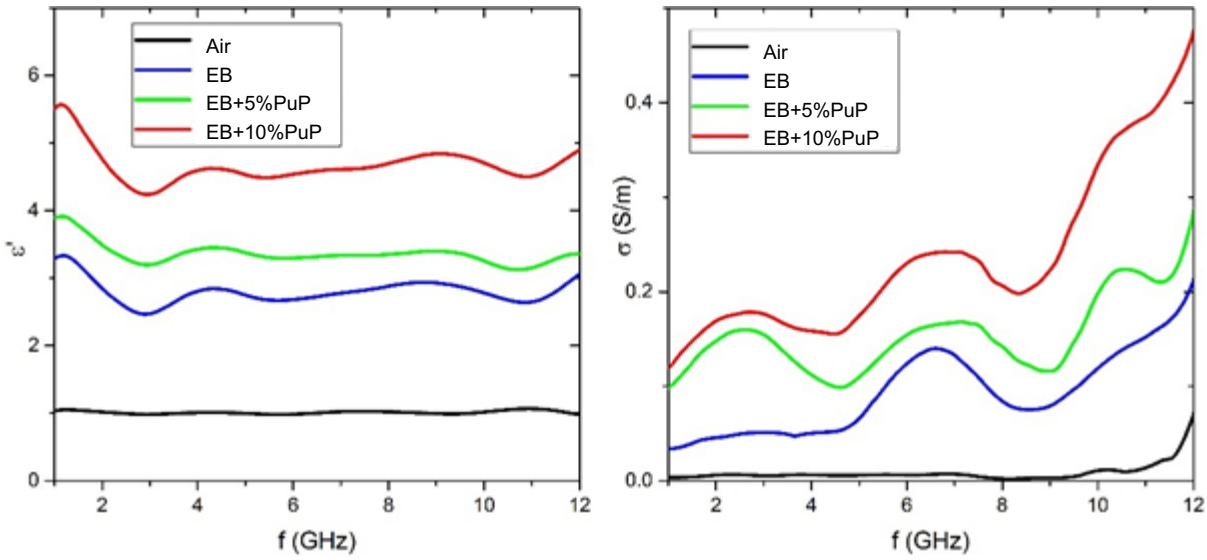

Figure 11. Real part of the complex dielectric permittivity (left) and conductivity (right) as a function of frequency in the S, C and X -bands for EB and EB-PuP samples. A measurement performed on air is shown for comparison. The bumps and ripples visible on all measurements are typical of high frequency characterization techniques based on coaxial cells and are not related to the materials properties.

4. Conclusions

Biochar-based particles derived from cellulose nanocrystals were successfully modified by growing carbon nanofibers onto their outer surface; the obtained porcupine-like structures were introduced in a UV-LED curable epoxy-acrylate resin aiming at achieving composite coatings with enhanced properties. Preliminary rheological analyses performed on the UV-LED curable dispersions containing different loadings of PuP particles showed a significant effect of the embedded carbonaceous structures on the material low-frequency behavior, suggesting the occurrence of strong interactions between the oligomeric chains and the carbon nanofibers of the PuP structures. Furthermore, the thermal characterization of the cured films demonstrated the completeness of the curing reactions also in presence of high loadings of PuP particles, thus indicating the effectiveness of the experimental conditions adopted for the UV-LED curing process. The introduction of the PuP structures did not affect the thermo-oxidative stability of the cured films; besides, progressively higher values of the storage modulus were obtained for the composite films containing increasing loadings of particles as compared to the unfilled counterpart. Finally, a monotonic increase of the thermal and electrical conductivity was observed as a function of the PuP particle loading.

References

[1] Y. Yagci, S. Jockusch, N.J. Turro, Photoinitiated Polymerization: Advances, Challenges, and Opportunities, Macromolecules 65 (2010) 6245-6260. https://doi.org/10.1021/ma1007545.

[2] C. Mendes-Felipe, J. Oliveira, I. Etxebarria, J.L. Vilas-Vilela, S. Lanceros-Mendez, State-of-the-Art and Future Challenges of UV Curable Polymer-Based Smart Materials for Printing Technologies, Adv. Mat. Technol. 4 (2019) 1800618. https://doi.org/10.1002/admt.201800618.

[3] A.C. Scranton, C.N. Bowman, R.W. Peier, Photopolymerization Fundamentals and Applications, ACS Symposium Series 673; American Chemical Society: Washington, 1997.

[4] S.C. Ligon-Auer, M. Schwentenwein, C. Gorsche, J. Stampfl, R. Liska, Toughening of photo-curable polymer networks: a review, Polym. Chem. 7 (2016) 257-286. https://doi.org/10.1039/C5PY01631B.

[5] C. Decker, Photoinitiated crosslinking polymerization, Prog. Polym. Sci. 21 (1996) 593-650. https://doi.org/10.1016/0079-6700(95)00027-5.

[6] C. Dietlin, S. Schweizer, P. Xiao, J. Zhang, F. Morlet-Savary, B. Graff, J.P. Fouassier, J. Lalevée, Photopolymerization upon LEDs: new photoinitiating systems and strategies, Polym. Chem. 6 (2015) 3895-3912. https://doi.org/10.1039/C5PY00258C.

[7] F. Galiano, S.A. Schmidt, X. Ye, R. Kumar, R. Mancuso, E. Curcio, B. Gabriele, J. Hoinkis, A. Figoli, UV-LED induced bicontinuous microemulsions polymerisation for surface modification of commercial membranes-Enhancing the antifouling properties, Sep. Purif. Technol. 194 (2018) 149-160. https://doi.org/10.1016/j.seppur.2017.10.063.

[8] V. Landry, P. Blanchet, G. Boivin, J.F. Bouffard, M. Vlad, UV-LED Curing Efficiency of Wood Coatings, Coatings 5 (2015) 1019-1033. https://doi.org/10.3390/coatings5041019.

[9] Z. Chu, Y. Feng, B. Xie, Y. Yang, Y. Hu, X. Zhou, T. Yuan, Z. Yang, Bio-based polyfunctional reactive diluent derived from tung oil by thiol-ene click reaction for high bio-content UV-LED curable coatings, Ind. Crop. Prod. 160 (2021) 113117. https://doi.org/10.1016/j.indcrop.2020.113117

[10] M. Faes, J. Vleugels, F. Vogeler, E. Ferraris, Extrusion-based additive manufacturing of ZrO_2 using photoinitiated polymerization, CIRP J. Manuf. Sci. Technol. 14 (2016) 28-34. https://doi.org/10.1016/j.cirpj.2016.05.002.

[11] X. Li, D. Wang, L. Zhao, X. Hou, L. Liu, B. Feng, M. Li, P. Zheng, X. Zhao, S. Wei, UV LED curable epoxy soybean-oil-based waterborne PUA resin for wood coatings, Prog. Org. Coat. 151 (2021) 105942. https://doi.org/10.1016/j.porgcoat.2020.105942.

[12] A. Javadi, H.S. Mehr, M. Sobani, M.D. Soucek, Cure-on-command technology: A review of the current state of the art, Progr. Org. Coat. 100 (2016) 2-31. https://doi.org/10.1016/j.porgcoat.2016.02.014.

[13] M.J. Sampaio, A. Benyounes, P. Serp, J.L. Faria, C.G. Silva, Photocatalytic synthesis of vanillin using N-doped carbon nanotubes/ZnO catalysts under UV-LED irradiation, Appl. Catal. A 551 (2018) 71-78. https://doi.org/10.1016/j.apcata.2017.12.002.

[14] S. Seipel, J. Yu, A.P. Periyasamy, M. Vikov´, M. Vik, V.A. Nierstrasz, Inkjet printing and UV-LED curing of photochromic dyes for functional and smart textile applications, RCS Adv. 8 (2018) 28395. https://doi.org/10.1039/C8RA05856C.

[15] S.K. Ghazali, N. Adrus, R.A. Majid, F. Ali, J. Jamaluddin, UV-LED as a New Emerging Tool for Curable Polyurethane Acrylate Hydrophobic Coating, Polymers 13 (2021) 487. https://doi.org/10.3390/polym13040487.

[16] G. Malucelli, Synthesis and Characterization of UV-LED Curable Nanocomposite Coatings, Curr. Org. Chem. 21 (2017) 1-8. https://doi.org/10.2174/1385272821666170307095213

[17] X. Wang, Y. Feng, L. Zhang, I. Protsak, R. Jamali, Y. Shu, P. Pal, Z. Wang, J. Yang, D. Zhang, Fast-cured UV-LED polymer materials filled with high mineral contents as wear-resistant, antibacterial coatings, Chem. Eng. J. 82 (2020) 122927. https://doi.org/10.1016/j.cej.2019.122927.

[18] V. Strongone, M. Bartoli, P. Jagdale, R. Arrigo, A. Tagliaferro, G. Malucelli, Preparation and Characterization of UV-LED Curable Acrylic Films Containing Biochar and/or Multiwalled Carbon Nanotubes: Effect of the Filler Loading on the Rheological, Thermal and Optical Properties, Polymers 12 (2020) 796. https://doi.org/10.3390/polym12040796.

[19] E. Behazin, M. Misra, A.K. Mohanty, Sustainable biocarbon from pyrolyzed perennial grasses and their effects on impact modified polypropylene biocomposites, Comp. Part B Eng. 118 (2017) 116-124. https://doi.org/10.1016/j.compositesb.2017.03.003.

[20] Q. Zhang, W. Yi, Z. Li, L. Wang, H. Cai, Mechanical Properties of Rice Husk Biochar Reinforced High Density Polyethylene Composites, Polymers 10 (2018) 286. https://doi.org/10.3390/polym10030286.

[21] R. Arrigo, M. Bartoli, G. Malucelli, Poly(lactic Acid)–Biochar Biocomposites: Effect of Processing and Filler Content on Rheological, Thermal, and Mechanical Properties, Polymers 12 (2020) 892. https://doi.org/10.3390/polym12040892.

[22] A. Tomczyk, Z. Sokołowska, P. Boguta, Biochar physicochemical properties: Pyrolysis temperature and feedstock kind effects, Rev. Environ. Sci. Biotechnol. 19 (2020) 191-215. https://doi.org/10.1007/s11157-020-09523-3.

[23] A.Y. Elnour, A.A. Alghyamah, H.M. Shaikh, A.M. Poulose, S.M. Al-Zahrani, A. Anis, M.I. Al-Wabel, Effect of Pyrolysis Temperature on Biochar Microstructural Evolution, Physicochemical Characteristics, and Its Influence on Biochar/Polypropylene Composites, Appl. Sci. 9 (2019) 1149. https://doi.org/10.3390/app9061149.

[24] D.R. Vardon, B.R. Moser, W. Zheng, K. Witkin, R.L. Evangelista, T.J. Strathmann, K. Rajagopalan, B.K. Sharma, Complete Utilization of Spent Coffee Grounds To Produce Biodiesel, Bio-Oil, and Biochar, ACS Sustain. Chem. Eng. 1 (2013) 1286-1294. https://doi.org/10.1021/sc400145w.

[25] M. Bartoli, M.A. Nasir, E. Passaglia, R. Spiniello, P. Jagdale, C. Rosso, M. Giorcelli, M. Rovere, A. Tagliaferro, Influence of pyrolytic thermal history on olive pruning biochar and related epoxy composites mechanical properties, J. Comp. Mat. 54 (2020) 1863-1873. https://doi.org/10.1177/0021998319888734.

[26] E. Singh, A. Kumar, R. Mishra, S. You, L. Singh, S. Kumar, R. Kumar, Pyrolysis of waste biomass and plastics for production of biochar and its use for removal of heavy metals from aqueous solution, Bioresour. Technol. 320 (2021) 124278. https://doi.org/10.1016/j.biortech.2020.124278.

[27] Q. Hu, J. Jung, D. Chen, K. Leong, S. Song, F. Li, B.C. Mohan, Z. Yao, A.K. Prabhakar, X. Lin, E. Lim, L. Zhang, G. Souradeep, Y. Ok, H. Kua, S. Li, H. Tan, Y. Dai, Y. Tong, Y. Peng, S. Josep, C. Wang, Biochar industry to circular economy, Sci. Total Environ. 757 (2021) 143820. https://doi.org/10.1016/j.scitotenv.2020.143820.

[28] M. Bartoli, M. Giorcelli, M. Rovere, P. Jagdale, A. Tagliaferro, M. Chae, D.C. Bressler, Shape tunability of carbonized cellulose nanocrystals, SN Appl. Sci. 1 (2019) 1661-1676. .

[29] M. Bartoli, M. Giorcelli, C. Rosso, M. Rovere, P. Jagdale, A. Tagliaferro, Influence of Commercial Biochar Fillers on Brittleness/Ductility of Epoxy Resin Composites, Applied Sciences 9 (2019) 13. https://doi.org/10.3390/app9153109.

[30] T. Log, S.E. Gustafsson, Transient plane source (TPS) technique for measuring thermal transport properties of building materials, Fire Mater. 19 (1995) 43-49. https://doi.org/10.1002/fam.810190107

[31] M. Giorcelli, M. Bartoli, Development of Coffee Biochar Filler for the Production of Electrical Conductive Reinforced Plastic, Polymers 11 (2019) 17. https://doi.org/10.3390/polym11121916.

[32] D. Ba, P. Sabouroux, Epsimu, a toolkit for permittivity and permeability measurement in microwave domain at real time of all materials: Applications to solid and semisolid materials, Microw. Opt. Technol. Lett. 52 (2010) 2643-2648. https://doi.org/10.1002/mop.25570.

[33] N.A.M. Radzuan, A.B Sulong, J. Sahari, A review of electrical conductivity models for conductive polymer composite, Int. J. Hydrog. Energy 42 (2017) 9262-9273. https://doi.org/10.1016/j.ijhydene.2016.03.045.

[34] A. Tagliaferro, M. Rovere, E. Padovano, M. Bartoli, M. Giorcelli, Introducing the Novel Mixed Gaussian-Lorentzian Lineshape in the Analysis of the Raman Signal of Biochar, Nanomaterials 10 (2020) 1748. https://doi.org/10.3390/nano10091748.

[35] F. Shafizadeh, Y. Sekiguchi, Development of aromaticity in cellulosic chars, Carbon 21 (1983) 511-516. https://doi.org/10.1016/0008-6223(83)90144-6.
[36] M.A. Signore, C. De Pascali, D. Duraccio, G. Malucelli, A. Fioravanti, E. Melissano, M.C. Martucci, M. Masieri, P. Siciliano, L. Francioso, Synthesis and characterization of UV-curable nanocellulose/ZnO/AlN acrylic flexible films: Thermal, dynamic mechanical and piezoelectric response, J. Appl. Polym. Sci. 138 (2021) 49731. https://doi.org/10.1002/app.49731.
[37] M.A. Bashir, Use of Dynamic Mechanical Analysis (DMA) for Characterizing Interfacial Interactions in Filled Polymers, Solids 2 (2021) 108-120. https://doi.org/10.3390/solids2010006.
[38] D. Fragiadakis, P. Pissis, Glass transition and segmental dynamics in poly(dimethylsiloxane) /silica nanocomposites studied by various techniques, J. Non-Cryst. Solids 353 (2007) 4344-4352. https://doi.org/10.1016/j.jnoncrysol.2007.05.183.
[39] M. Giorcelli, M. Bartoli, A. Sanginario, E. Padovano, C. Rosso, M. Rovere, A. Tagliaferro, High-Temperature Annealed Biochar as a Conductive Filler for the Production of Piezoresistive Materials for Energy Conversion Application, ACS Appl. Electron. Mater. 3 (2021) 838-844. https://doi.org/10.1021/acsaelm.0c00971.

Highlights

- Composite coatings based on a UV-LED curable epoxy-acrylate resin were formulated
- Porcupine-like particles based on biochar and carbon nanofibers were used as fillers
- UV-LED cured composite films show improved dynamic-mechanical properties
- The thermo-oxidative stability of the cured films is not affected by PuP structures
- Improved thermal and electrical conductivities were achieved for the composite films